



# **Geophysical Research Letters**\*



### RESEARCH LETTER

10.1029/2024GL113933

#### **Key Points:**

- The highest values of spectral curvature between 300 and 600 nm map the youngest geological features of Mercury
- The spectral curvature on Mercury is well preserved near the cold poles and affected by thermal weathering near the hot poles

#### **Supporting Information:**

Supporting Information may be found in the online version of this article.

#### Correspondence to:

O. Barraud, oceane.barraud@dlr.de

#### Citation:

Barraud, O., Besse, S., D'Amore, M., & Helbert, J. (2025). Impact of thermal weathering on mercury's reflectance. *Geophysical Research Letters*, 52, e2024GL113933. https://doi.org/10.1029/2024GL113933

Received 26 NOV 2024 Accepted 30 MAR 2025

#### **Author Contributions:**

Formal analysis: O. Barraud,

M. D'Amore
Methodology: O. Barraud, S. Besse,
J. Helbert
Supervision: J. Helbert
Visualization: O. Barraud, M. D'Amore
Writing – original draft: O. Barraud
Writing – review & editing: S. Besse,
M. D'Amore. J. Helbert

Conceptualization: O. Barraud, S. Besse

© 2025. The Author(s). This is an open access article under the terms of the Creative Commons Attribution License, which permits use, distribution and reproduction in any medium, provided the original work is properly cited.

## **Impact of Thermal Weathering on Mercury's Reflectance**

O. Barraud<sup>1</sup>, S. Besse<sup>2</sup>, M. D'Amore<sup>1</sup>, and J. Helbert<sup>1,3</sup>

<sup>1</sup>German Aerospace Center (DLR) - Institute of Planetary Research, Berlin, Germany, <sup>2</sup>ESA/ESAC, Villanueva de la Cañada, Spain, <sup>3</sup>ESA/ESTEC, Noordwijk, The Netherlands

**Abstract** MErcury Surface, Space ENviroment, GEochemistry, and Ranging (MESSENGER) observations suggest that sulfur-bearing minerals are key components of Mercury's surface. These minerals have been proposed to explain the strong concave downward curvature between 300 and 600 nm in MESSENGER reflectance spectra of the hollows. We investigated the spectral curvature of the entire surface of Mercury and its relationship with surface temperature. High spectral curvatures map the youngest terrains: hollows, bright spots and very bright craters within the Mercury cold poles. These results demonstrate that freshly exposed materials are spectrally similar to hollows-forming material and sulfides. High spectral curvature is muted by thermal processing near Mercury's hot poles. The optical effect of thermal weathering that we observed on Mercury are consistent with laboratory measurements on weathered CaS and includes a flattening of the reflectance in the visible. This suggests Mercury's crustal composition to be rich in sulfur-bearing minerals.

Plain Language Summary Reflectance measurements are used to investigate the composition, alteration and physical properties of planetary surfaces. On Mercury, spectroscopic observations from previous missions lack asbsorption features to identified minerals. However, the overall shape of the spectrum in the near-ultraviolet to near-infrared is used to differentiate the different terrains types and spectral units. Here, we investigated the spectral curvature—that is, the concavity - of Mercury in the near-ultraviolet to visible. We found that the temperature and aging of the surface strongly alter this spectral property previously related to surface composition only.

### 1. Introduction

Spectral reflectance is a key measurement for investigating the composition and space weathering processes of airless planetary bodies. On the Moon and Mercury, space weathering alters spectral signatures at visible (VIS) to near-infrared (NIR) wavelengths by (a) darkening (lowering the spectral albedo), (b) reducing spectral contrast (decreasing the strength of absorption features), and (c) reddening of the spectrum (increasing the slope of the continuum reflectance with increasing wavelength) (e.g., Fischer & Pieters, 1994; McCord & Adams, 1972a, 1972b; Pieters & Noble, 2016; Vilas, 1985). These spectral changes are the results of the production of submicroscopic iron-metal particles (e.g., Hapke, 2001; Lucey & Riner, 2011), the formation of impact glasses and agglutinates (e.g., Hörz & Cintala, 1997), and the physical fragmentation of regolith into finer grains (e.g., Pieters et al., 1993). Because of Mercury's proximity to the Sun, space weathering processes such as irradiation, impact gardening and thermal weathering are expected to be significantly stronger and the formation of space weathering products faster (e.g., Cintala, 1992; Domingue et al., 2014; Noble & Pieters, 2003; Pieters & Noble, 2016). The MErcury Surface, Space ENviroment, GEochemistry, and Ranging (MESSENGER) mission provided the most complete in-situ dataset of spectroscopic observations of Mercury's surface and therefore information on Mercury's space weathering products. The Visible and InfraRed Spectrograph (VIRS), the surface component of the Mercury Atmospheric and Surface Composition Spectrometer (MASCS) (McClintock & Lankton, 2007), sampled Mercury's reflectance in the wavelength domain from 300 to 1,450 nm with a spectral resolution of 5 nm. Spectroscopic observations of Mercury's surface lack absorption features of mafic minerals such as pyroxene or olivine (Izenberg et al., 2014; Murchie et al., 2015). However, fresh material exhibits a higher spectral albedo and less red continuum slope (Blewett et al., 2009; Domingue et al., 2014; Izenberg et al., 2014; McClintock et al., 2008; Murchie et al., 2015; Robinson et al., 2008). Brightest units on Mercury are fresh craters and hollows (Murchie et al., 2015). Fresh craters exhibit bright ejecta rays and crisp morphology and are dated to Kuiperianage (<1 Ga) (Blewett et al., 2018; Murchie et al., 2015). Hollows have been dated by crater counting or by dating their host craters to very recent time: around hundreds of thousands of years (Blewett et al., 2018; Wang et al., 2020). Multispectral images from the MDIS/WAC (Mercury Dual Imaging System Wide Angle Camera)

BARRAUD ET AL. 1 of 10

(Hawkins et al., 2007) camera revealed, in addition to reflectance levels higher by twice the average surface of Mercury, that some hollows exhibit a weak absorption feature centered around 630 nm (Lucchetti et al., 2018, 2021; Vilas et al., 2016). Sulfides (Vilas et al., 2016), chlorides (Lucchetti et al., 2021), or a mix of pyroxenes and sulfides (Lucchetti et al., 2018) or graphite and sulfides (Vilas et al., 2016) are commonly proposed to explain this absorption feature. Mercury Atmospheric and Surface Composition Spectrometer/VIRS spectroscopic measurements of several hollows do not exhibit such an absorption feature (Barraud et al., 2020). Moreover, MASCS/ VIRS spectra of hollows exhibit a strong concave downward curvature between 300 and 600 nm that makes it possible to spectrally differentiate the hollows from several other spectral and/or geological units (Barraud et al., 2020). Comparison with laboratory spectra of Mercury analogue minerals shows that sulfides and/or chlorides are the best compounds to explain the curvature of hollows (Barraud et al., 2023). The hollows spectral curvature is approximately 3-4 times higher than the spectral curvature of the Low-reflectance Material (LRM, dark material enriched in carbon, Klima et al., 2018) and High-reflectance Red Plains (HRP, products of effusive volcanism) (Barraud et al., 2020). Here, we performed an analysis of the spectral curvature at the planet scale. Our main objectives are (a) identify the geological features with the highest values of curvature and (b) investigate their spatial distribution. We then discuss the relationship between spectral curvature, composition, and space weathering, especially the thermal processing of the surface.

#### 2. Dataset and Methods

Mercury Atmospheric and Surface Composition Spectrometer/VIRS is composed of two detectors: a visible (VIS) detector operating between 300 and 1,050 nm and a NIR detector sensitive to wavelengths between 900 and 1,450 nm (McClintock & Lankton, 2007). In this study, only the reflectance measured by the VIS detector is used. We downloaded the VIRS Derived Data Record (DDR) data products available on the Planetary Data System (PDS) radiometrically and photometrically calibrated by the MESSENGER team. Additional processing is applied to the DDR data by first removing the outliers deviating by more than 2 sigma (less than 1% of the VIS channels) and then smoothing the spectrum by an average window of three points.

In order to obtain the better MASCS/VIRS dataset, the data are filtered by instrument temperature (see Supporting Information S1) and incidence angle. The data recorded in the highest temperature regime of the instrument (temperature exceeding 40°C) are removed in order to avoid the possible effect of high instrument temperatures on the reflectance. Illumination and viewing geometry affect the spectral reflectance which is more sensitive to the effects of topography at high phase angles. MASCS/VIRS spectra obtained at incidence angles higher than 75° are discarded from the study. This work, which includes around 14,000 observations of MASCS/VIRS, allows us to identify observations with strong increase or drop off in reflectance at the edges of the VIS detector wavelength domain. The signal-to-noise ratio (SNR) of the VIS detector decreases after 800 nm (Besse et al., 2015; Holsclaw et al., 2010; Izenberg et al., 2014). Therefore, some of the MASCS/VIRS spectra exhibit strong reflectance variability beyond 800 nm. However, we also identified spectra with a strong increase of reflectance at the shorter wavelengths (UV domain) of the VIS detector. The reason for these variations remains undefined, however, they may be due to changes of instrument sensitivity, artifacts of the instrument or introduced during calibration. Therefore we decided to remove all the MASCS/VIRS spectra that contain strong variation of reflectance at the boundaries of the detector (before 350 nm and after 800 nm). For this purpose, we calculated three slope ratios across the VIS detector wavelength range:

$$UV1 = S_{300-350}/S_{250-300}$$

$$UV2 = S_{300-350}/S_{350-500}$$

$$VIS = S_{700-900}/S_{500-700}$$

Each slope  $S_{\lambda 1 - \lambda 2}$  is calculated by a linear fit across the wavelength range  $\lambda 1$  to  $\lambda 2$  in nm (see Figure S1 in Supporting Information S1).

Spectra are used in this study if the UV1 ratio is strictly higher than 0 and lower than 1.5, the UV2 ratio is strictly higher than 0 and lower than 3.5 and the VIS ratio is strictly higher than 0 and lower than 2. These values have been defined empirically based on the sub-dataset of around 14,000 spectra and removed around 10% of the sub-dataset. Some examples are shown in Figure S1 in Supporting Information S1.

BARRAUD ET AL. 2 of 10

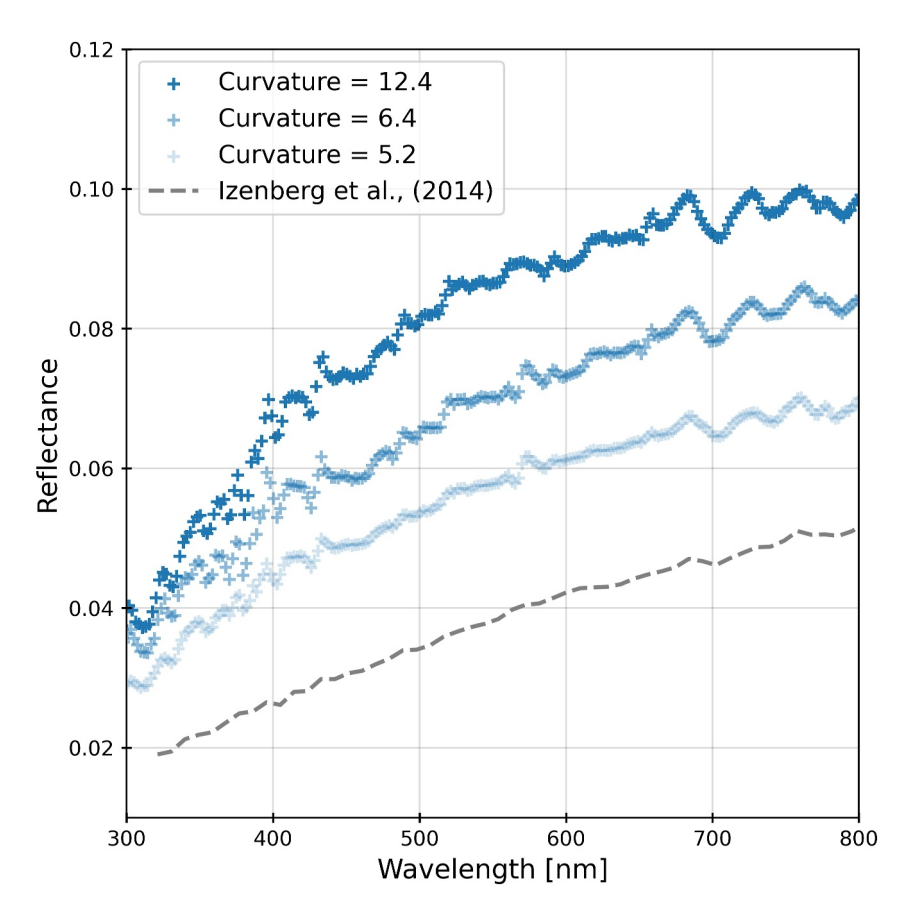


**Figure 1.** Mercury Atmospheric and Surface Composition Spectrometer/Visible and InfraRed Spectrograph spectra between 300 and 800 nm with various values of spectral curvature. The curvature is normalized to the reference spectrum (Izenberg et al., 2014) in gray. The reference spectrum has a curvature value of 1 and is almost linear between 300 and 600 nm.

After applying the filtering, we calculated the curvature parameter as defined in Figure 1 of Barraud et al. (2020). The curvature parameter corresponds to the coefficient of the squared power of the polynomial fit (degree 2) of the spectrum between 300 and 600 nm:

Reflectance = 
$$c\lambda^2 + b\lambda + a$$
 (c = curvature)

The curvature (coefficient of the squared power of the polynomial fit) is then normalized to the curvature of an average spectrum of 850,000 spectra of Mercury's surface (Izenberg et al., 2014). Thus, curvature parameter equals to one is representative of Mercury's mean surface. Barraud et al. (2020) showed that the curvature parameter ranges between around -5 and 5 in LRM and HRP and from around 2 to 7 in the faculae analyzed by Barraud et al. (2021). For the hollows, the curvature parameter ranges from 5 to 17 (Barraud et al., 2020, 2023). Therefore, in this study we selected the MASCS/VIRS observations with a curvature parameter higher than five in order to map the geological units with curvature values comparable to the hollows or higher. Figure 1 shows artifact-free spectra in the visible domain with various values of the curvature parameter.

### 3. Results

Artifact-free observations with high curvature represent 11,834 footprints (Figure 2), that is, 0.32% of the MASCS/VIRS data obtained under the best instrumental conditions. These 11,834 footprints map 693 different features on Mercury's surface. We classified these features in 6 categories using the MDIS/WAC global base map at a spatial resolution of 166 m/pixel (which is in average 30 times better than the MASCS spatial resolution): hollows, bright spots, very bright craters, crater rims, crater floors, and faculae (Figure 3). Features are classified as hollows when MASCS/VIRS footprints are in a region/crater where hollows have been mapped by Thomas

BARRAUD ET AL. 3 of 10

2025, 9, Downloaded from https://agupubs.onlinelibrary.wiley.com/doi/10.1029/2024GL113933 by Disch Zentrum F. Luft-U. Raum Fahrt In D. Helmholtz Gemein., Wiley Online

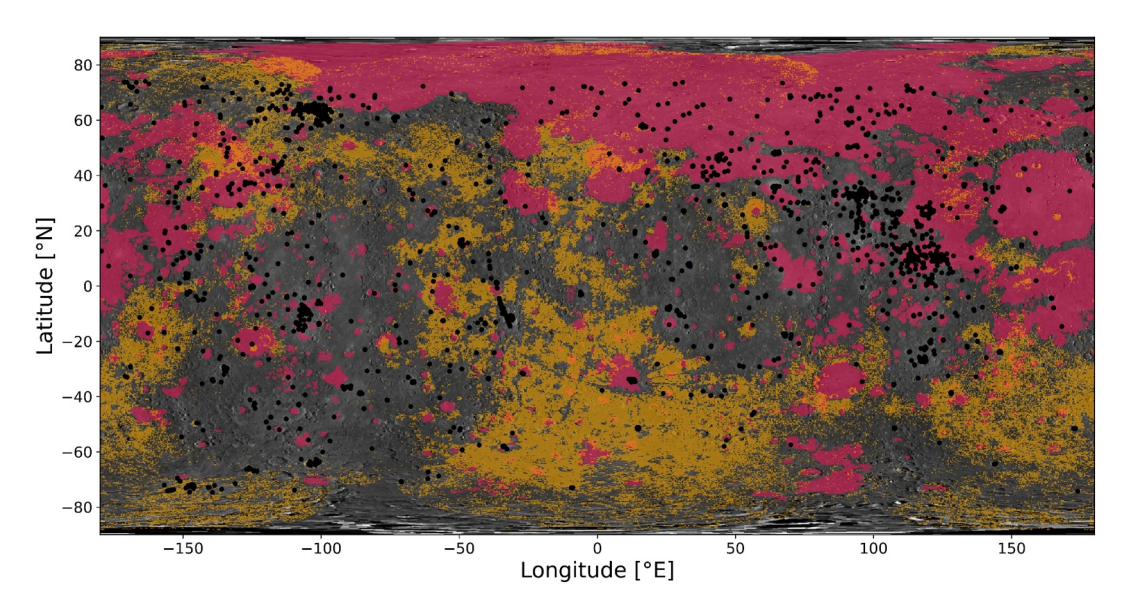


**Figure 2.** Distribution of high spectral curvature on Mercury's surface. The figure shows the 11,834 Mercury Atmospheric and Surface Composition Spectrometer/Visible and InfraRed Spectrograph footprints with curvature value higher than 5 between 300 and 600 nm (black dots). The size of the dots is not the size of the footprints. The background mosaic is the MDIS/WAC global base map (166 m/pixel) used for the classification. Mercury's smooth plains (Denevi et al., 2013) are highlighted in pink and the Low-reflectance Material (Klima et al., 2018) are highlighted in orange.

et al. (2014a) (Figure 3a). Impact craters with a diameter smaller than 10 km or bright regions smaller than 10 km (without visible impact crater at the MDIS/WAC base map spatial resolution) with reflectance level comparable to fresh impact craters (reflectance at 750 nm > 0.06) are classified as bright spots (Figure 3b). Craters larger than 10 km in diameter with fresh morphology and bright ejecta are classified as very bright craters (Figure 3c). Units located inside craters with a diameter higher than 10 km without fresh and bright ejecta are classified in two different categories according to their location inside the crater. Features located on the crater rims/walls are classified as "crater rims" while features located inside the floor and impact structures such as peak rings or central peaks are classified as "crater floors" (Figures 3d and 3e). Finally, features located inside previously identified faculae and/or volcanic pits (Thomas et al., 2014b) are classified as faculae (Figure 3f).

Among the 693 features, 73% represent the youngest features on Mercury: bright spots, hollows and very bright craters (Figure 4a) (e.g., Blewett et al., 2009, 2018; Robinson et al., 2008). 25% of the features are located in crater floors or crater rims without previously identified hollows but many of these locations include craters with wall collapses or overlying secondary craters which might have been responsible for the exposure of fresh materials. Recent work on the localization of hollows inside impact craters indicates that a significant percentage of hollows are formed within superposed impact craters which might be key drivers in excavating hollow-forming volatiles (Giroud-Proeschel et al., 2024). Around 2% of the features are classified as faculae. All the footprints inside faculae are located in or cover part of the volcanic pits. Analysis of MDIS images inside the Lermontov crater have shown some hollows inside volcanic pits (Pajola et al., 2021). Galiano et al. (2023) identified MASCS/VIRS spectra with a different behavior from faculae inside the volcanic vents of Nathair Facula and Picasso impact crater. The high curvature detected inside the volcanic pits may be therefore due to other geological units such as hollows or freshly exposed material inside the pits. Among the hollows mapped by Thomas et al. (2014a), 14% are mapped in this study. This relatively low percentage of hollows mapped may be explained easily by the low coverage of the MASCS/VIRS instrument which strongly decreases the probability to observe small features such as the hollows. The spatial resolution of MASCS/VIRS footprints is generally inadequate for the size (few hundreds of km to several km) of small geological units (hollows, bright spots, etc.).

The features with high curvature are not found preferentially in one major geological or global spectral unit. They are found inside smooth plains, LRM (Klima et al., 2018), large basins such as Caloris, and intercrater plains (Figure 2). The longitudinal distribution of those features with high curvature is shown in the histogram in

BARRAUD ET AL. 4 of 10

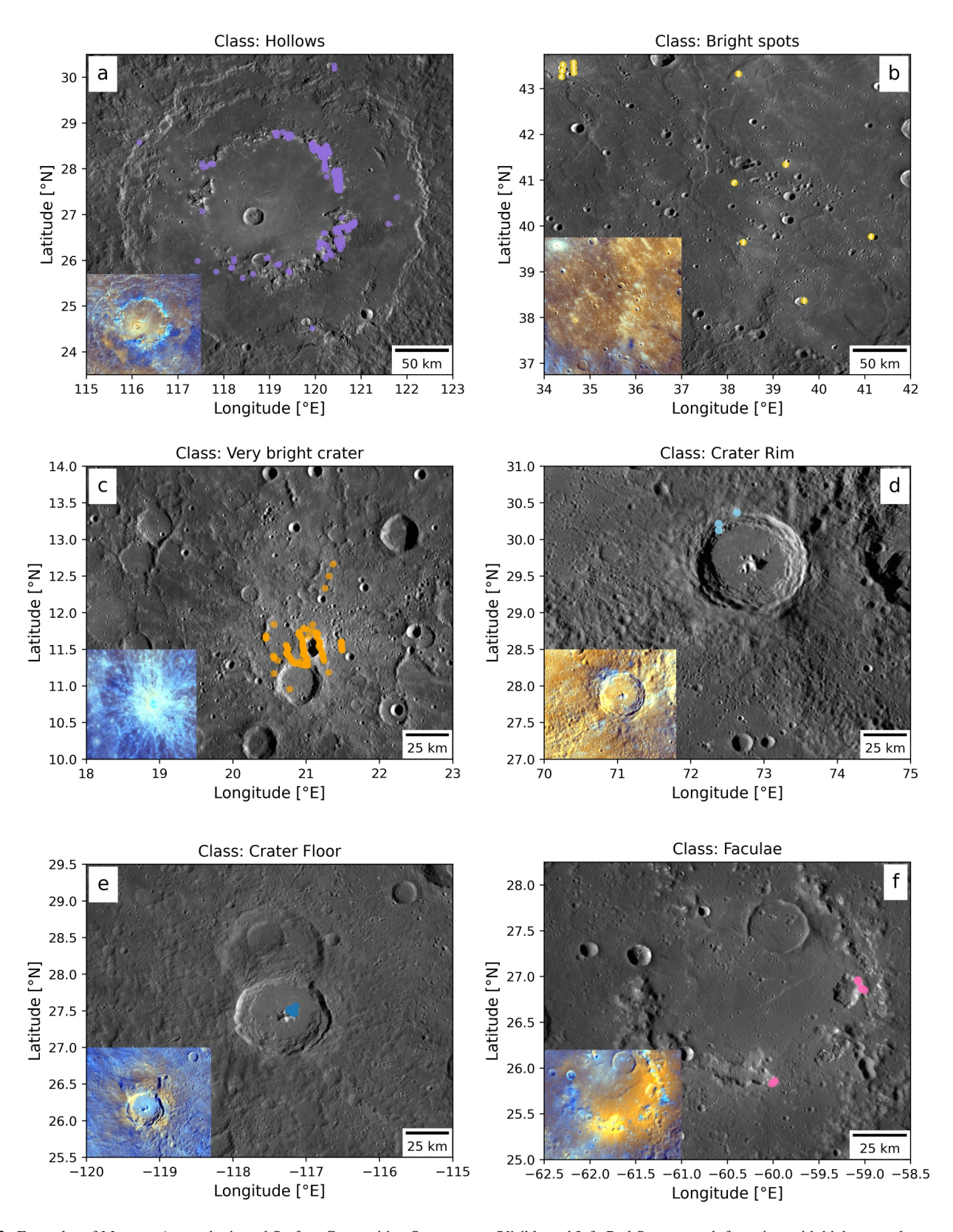


**Figure 3.** Examples of Mercury Atmospheric and Surface Composition Spectrometer/Visible and InfraRed Spectrograph footprints with high spectral curvature mapping 6 classes of geological units. The footprints are smaller than the size of the dots. The background mosaic is the MDIS/WAC global base map (166 m/pixel) used for the classification. The MDIS/WAC enhanced color mosaic (R: second principal component, G: first principal component, B: 430 nm/1000 nm ratio) shows the MDIS spectral variation of each region.

BARRAUD ET AL. 5 of 10

wiley.com/doi/10.1029/2024GL113933 by Dtsch Zentrum F. Luft-U. Raum Fahrt In D. Helmholt

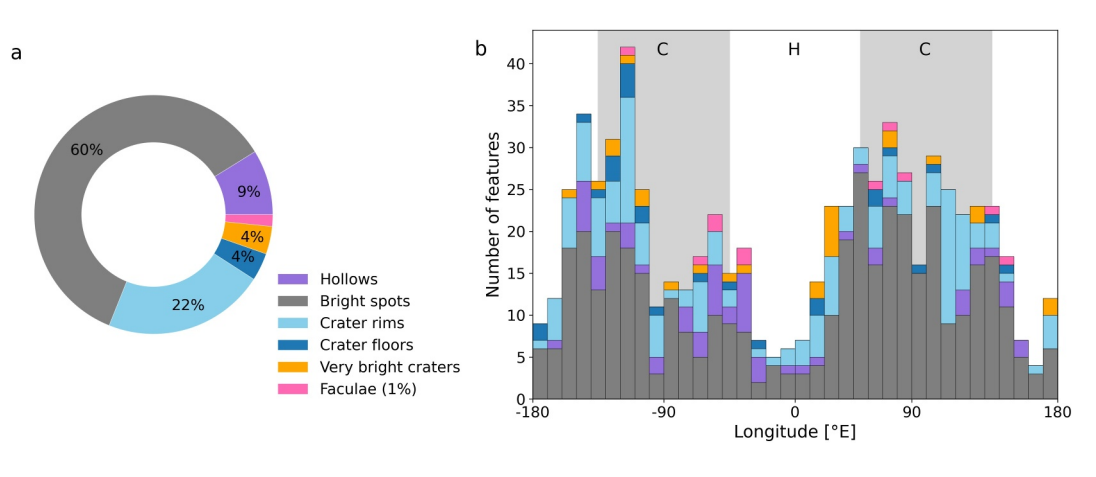


**Figure 4.** (a) Percentage of high curvature features in each class, and (b) longitudinal distribution of the features with high curvature values. The gray shaded regions show Mercury's cold poles (C) and the white regions show Mercury's hot poles (H). The color code is the same between the two panels. The features are mainly concentrated around Mercury's cold poles.

Figure 4b. Due to the orbital parameters of Mercury (obliquity, resonance, rotation period), its surface undergoes large temperature variations. Thermal modeling predicts the presence of "cold" poles around 90°E and -90°E and "hot" poles around 0°E and 180°E (Bauch et al., 2021). At cold poles longitudes, the surface temperatures reach 560 K on equatorial latitudes at local noon while at hot poles longitudes the surface temperature reaches 700 K at local noon around the equator (Bauch et al., 2021). In our study, the highest occurrence of high spectral curvature features is observed at longitudes around the cold poles (Figure 4b). An in-depth study of the MASCS/VIRS dataset shows no instrument or observational bias in the longitudinal distribution of the high curvature features (see Supporting Information S1). The hollows, bright spots, and faculae are not preferentially found around the Mercury's cold or hot poles but occur widely across Mercury (e.g., Kerber et al., 2011; Klima et al., 2013; Thomas et al., 2014a) which confirms that the distribution of the mapped features around the cold poles is mainly due to their spectral curvature and not biased by the occurrence of these geological units across Mercury. In addition, the smallest hollows are concentrated in colder terrains excluding observational bias due to the spatial resolution in the longitudinal distribution of their detections (Thomas et al., 2014a). These results demonstrate a strong correlation between the curvature of Mercury's reflectance spectra and the extreme temperature regime of its surface.

### 4. Implications for Composition and Thermal Weathering

The spectral curvature in the visible has been described by Barraud et al. (2023) as a composition effect by analyzing hollows spectra. Comparison with laboratory measurements (e.g., Varatharajan et al., 2019) shows that the best analogs to reproduce the high spectral curvature of MASCS/VIRS spectra are CaS, Na<sub>2</sub>S, MgS, CaCl<sub>2</sub> and MgCl<sub>2</sub> (Barraud et al., 2023). In fact, spectral modeling shows that the hollows spectra can be reproduced by adding sulfides and/or chlorides to the background material of the hollows (Barraud et al., 2023). Here, the high curvature spectra are not limited to hollows but mainly map the brightest and youngest features of Mercury: hollows, bright spots and very bright craters. This result demonstrates a relationship between spectral curvature in the visible and the age of the sampled features. Fresh/young impact craters at Mercury's surface therefore expose fresh material with a composition similar to that of the hollows.

MESSENGER observations with the *X*-Ray spectrometer (XRS) revealed that the Mercury surface is enriched in volatile elements such as Cl and S compared to the surface of the Moon (e.g., Nittler et al., 2018). *X*-Ray spectrometer observations have shown that there is a ubiquitous correlation between the concentrations of S and Ca on Mercury's surface (Nittler et al., 2011; Weider et al., 2012, 2014, 2015) interpreted as evidence for an abundance of Ca-bearing sulfide minerals (e.g., oldhamite) (Nittler et al., 2011; Weider et al., 2012, 2014). By combining the results obtained from MASCS/VIRS (Barraud et al., 2020, 2023) and XRS (Nittler et al., 2011; Weider et al., 2012, 2014) instruments, CaS appears to be the best candidate as fresh material exposed by young geological units (hollows, bright spots, very bright craters) with a high spectral curvature.

The features mapped in this study, hollows, bright spots, faculae, and very bright craters are widely found on Mercury's surface (e.g., Klima et al., 2013; Thomas et al., 2014a, Thomas et al., 2014b) yet in this study the high

BARRAUD ET AL. 6 of 10

curvature values are found preferentially in the cold poles. The spatial distribution of the high curvature values around the cold poles demonstrates the major role played by thermal weathering in the behavior of this spectral characteristic. The spectral curvature of MASCS/VIRS observations seems strongly affected by high temperature (700 K) around the hot poles. Laboratory measurements on thermally processed sulfides (Helbert et al., 2013; Varatharajan et al., 2019) have shown changes in their overall spectral characteristics compared to fresh sulfides in the visible to NIR (slopes, reflectance level, contrast of spectral signatures). However, the spectral properties of each sulfide behave differently to the thermal processing under Mercury's surface temperature (773 K during 30 min) (Helbert et al., 2013; Varatharajan et al., 2019). For example, MgS is slightly brighter and shows a more blueish (reflectance decreasing with increasing wavelength) continuum after thermal processing while CaS is darker and slightly redder (Helbert et al., 2013). The curvature parameter of some sulfides measured by Varatharajan et al. (2019) before and after thermal processing has been calculated by Barraud et al. (2023). The curvature of CaS and MgS is reduced after the thermal processing while the curvature of Na<sub>2</sub>S increases after thermal processing. The thermal stability of chlorides, such as MgCl<sub>2</sub> and CaCl<sub>2</sub>, is unknown. These compounds are also good candidates for explaining the spectral curvature in the extreme surface environment of Mercury. However, following the current hypothesis that S and Ca are mainly under the state of CaS at the surface of Mercury (Nittler et al., 2011; Weider et al., 2012, 2014) the thermal processing at the temperature of the hot poles may explain the detection of high curvature values mainly around Mercury's cold poles. Oldhamite exposed by the youngest features (hollows, bright spots and very bright craters) may therefore have its curvature muted by the extreme temperature regime at Mercury's hot poles and would therefore no longer be spectrally detectable in these regions. The hypothesis of CaS is compatible with recent analysis of MDIS and Mercury Laser Altimeter data that shows a decrease in reflectance by 7%-12% in the hot poles compared to the 90°E cold pole in the low to midlatitudes (Deutsch et al., 2024). As mentioned previously, CaS is darker after thermal processing at the temperature of Mercury's hot poles (Helbert et al., 2013; Varatharajan et al., 2019). However, spectral curvature of CaS appears to be more affected by thermal weathering than reflectance at about 750 nm (Varatharajan et al., 2019; Barraud et al., 2023 Figure S1 in Supporting Information S1) which can explain why bright features are ubiquitously observed across Mercury.

Deutsch et al. (2024) suggests that the relatively lower reflectance of the hot poles may be the result of Ostwald ripening process by which nanophase Fe-metal particles coalesce and grow into larger particles at high temperatures (e.g., Noble et al., 2007; Noble & Pieters, 2003). Trang et al. (2017) investigated the amount of nanophase and microphase particles needed to model the MASCS/VIRS spectra by using radiative transfer modeling (e.g., Hapke, 2001; Lucey & Riner, 2011). They assumed that the regolith of Mercury consists of a silica matrix (i.e., the host material) with a constant reflectance of ~80% throughout the visible and NIR domain and add different mixtures of nanophase to microphase particles of Fe and C to fit the MASCS/VIRS spectra. The mean submicroscopic Fe abundance derived from Trang et al. (2017) model to reproduce MASCS/VIRS spectra exceeds the range of the XRS- and Gamma Ray Spectrometer-derived Fe estimates. They suggest that this result is due to assumptions about the composition of the host material and propose to improve the results by including darker minerals such as sulfides or graphite. The optical effects of space weathering may therefore be explained by a combination of weathered sulfides, such as CaS, and submicroscopic Fe particles. The addition of CaS in the model would therefore reduce the submicroscopic Fe content needed to darken and flatten the Mercury's spectra and fit with MESSENGER elemental data. Consequently, the optical effects of space weathering are not only a darkening and reddening of the spectra, as demonstrated in previous studies (e.g., Blewett et al., 2009; Domingue et al., 2014; Izenberg et al., 2014; McClintock et al., 2008; Murchie et al., 2015; Robinson et al., 2008), but also a flattening of the spectra between 300 and 600 nm, as demonstrated here.

### 5. Conclusions

Mercury's surface is iron-poor and undergoes extreme weathering which complicate the investigation of surface mineralogy by spectroscopic observations. Previous analyses show that the youngest features on Mercury exhibit higher albedo and less red spectral continuum. Here, we investigated the spectral curvature of Mercury's spectra between 300 and 600 nm, previously reported as a spectral characteristic of hollows. We showed that high curvature values map the youngest features at the surface of Mercury: hollows, bright spots and very bright craters. This result demonstrates a ubiquitous correlation between the spectral curvature and the freshness of the surface.

BARRAUD ET AL. 7 of 10

Furthermore, we investigated the spatial distribution of the high curvature features at the surface of the planet. We found that the highest occurrences of features with high spectral curvature are located at longitudes around 90°E and -90°E. The extreme thermal environment of Mercury and its peculiar orbit around the sun imply that the so-called Mercury's hot poles (0°E and 180°E) experience temperatures around 700 K over the course of a day. Our results demonstrate that around Mercury's cold poles (-90°E and 90°E, 560 K) the spectral curvature is less affected by thermal weathering while around the hot poles the curvature is muted and not detectable even on what appear to be fresh and recent geological features.

Previous work on the spectral curvature of the hollows demonstrated that this spectral feature is related to composition and especially the presence of sulfides and/or chlorides. Our results therefore lead us to the conclusion that bright spots and very bright craters exposed fresh material similar to the hollows-forming material and that thermal weathering reduced the curvature of this material. MESSENGER observations (spectral and chemical) suggest that oldhamite (CaS) is the best candidate to explain this spectral behavior. Laboratory measurements on CaS after thermal processing at Mercury's hot poles temperatures are consistent with our results and show a darkening, reddening and flattening between 300 and 600 nm of the spectra after heating. We demonstrated that thermal weathering played a major role in the behavior of visible reflectance on Mercury and must be considered when attempting to determine planet surface composition from remote sensing observations. Our study also demonstrates that laboratory investigations of thermally processed minerals are crucial for the future interpretation of BepiColombo observations.

### **Data Availability Statement**

The data used in this study are available at the PDS Geosciences Node of Washington University, St. Louis, MO, USA. The dataset used contains the latest calibration provided by the MESSENGER science team (https://pdsgeosciences.wustl.edu/missions/messenger/mascs.htm).

#### References

Barraud, O., Besse, S., & Doressoundiram, A. (2023). Low sulfide concentration in Mercury's smooth plains inhibits hollows. *Science Advances*, 9(12), eadd6452. https://doi.org/10.1126/sciadv.add6452

Barraud, O., Besse, S., Doressoundiram, A., Cornet, T., & Munoz, C. (2021). Spectral investigation of Mercury's pits' surroundings: Constraints on the planet's explosive activity. *Icarus*, 370, 114652. https://doi.org/10.1016/j.icarus.2021.114652

Barraud, O., Doressoundiram, A., Besse, S., & Sunshine, J. M. (2020). Near-ultraviolet to near-infrared spectral properties of hollows on Mercury: Implications for origin and formation process. *Journal of Geophysical Research: Planets*, 125(12), e2020JE006497. https://doi.org/10.1029/2020JE006497

Bauch, K. E., Hiesinger, H., Greenhagen, B. T., & Helbert, J. (2021). Estimation of surface temperatures on Mercury in preparation of the MERTIS experiment onboard BepiColombo. *Icarus*, 354, 114083. https://doi.org/10.1016/j.icarus.2020.114083

Besse, S., Doressoundiram, A., & Benkhoff, J. (2015). Spectroscopic properties of explosive volcanism within the Caloris basin with MESSENGER observations. *Journal of Geophysical Research: Planets*, 120(12), 2102–2117. https://doi.org/10.1002/2015JE004819

Blewett, D. T., Ernst, C. M., Murchie, S. L., & Vilas, F. (2018). Mercury's hollows. In S. C. Solomon (Ed.), *The view after MESSENGER* (pp. 324–345). Mercury.

Blewett, D. T., Robinson, M. S., Denevi, B. W., Gillis-Davis, J. J., Head, J. W., Solomon, S. C., et al. (2009). Multispectral images of Mercury from the first MESSENGER flyby: Analysis of global and regional color trends. *Earth and Planetary Science Letters*, 285(3–4), 272–282. https://doi.org/10.1016/j.epsl.2009.02.021

Cintala, M. J. (1992). Impact-induced thermal effects in the lunar and Mercurian regoliths. *Journal of Geophysical Research*, 97(E1), 947–973. https://doi.org/10.1029/91JE02207

Denevi, B. W., Ernst, C. M., Meyer, H. M., Robinson, M. S., Murchie, S. L., Whitten, J. L., et al. (2013). The distribution and origin of smooth plains on Mercury. *Journal of Geophysical Research: Planets*, 118(5), 891–990. https://doi.org/10.1002/jgre.20075

Deutsch, A. N., Neumann, G. A., Kreslavsky, M. A., Pokorný, P., Camacho, J. M. M., Trang, D., et al. (2024). Temperature-related variations of 1064 nm surface reflectance on Mercury: Implications for space weathering. *The Planetary Science Journal*, 5(1), 8. https://doi.org/10.3847/PSJ/ad0e6d

Domingue, D. L., Chapman, C. R., Killen, R. M., Zurbuchen, T. H., Gilbert, J. A., Sarantos, M., et al. (2014). Mercury's weather-beaten surface: Understanding Mercury in the context of lunar and asteroidal space weathering studies. *Space Science Reviews*, 181(1–4), 121–214. https://doi.org/10.1007/s11214-014-0039-5

Fischer, E. M., & Pieters, C. M. (1994). Remote determination of exposure degree and iron concentration of lunar soils using VIS-NIR spectroscopic methods. *Icarus*, 111(2), 475–488. https://doi.org/10.1006/icar.1994.1158

Galiano, A., Capaccioni, F., Filacchione, G., & Carli, C. (2023). Principal Component Analysis applied on MASCS/MESSENGER data for the spectral investigation of Mercury's surface. *Icarus*, 401, 115609. https://doi.org/10.1016/j.icarus.2023.115609

Giroud-Proeschel, E., Johnson, C. L., & Jellinek, A. M. (2024). The role of impact cratering in hollow formation on Mercury's surface: Hollow locations inside craters of different degradation indices. *LPI Contribution*, 3040, 2393.

Hapke, B. (2001). Space weathering from Mercury to the asteroid belt. Journal of Geophysical Research, 106(E5), 10039–10073. https://doi.org/ 10.1029/2000JE001338

Hawkins, S. E., III, Boldt, J. D., Darlington, E. H., Espiritu, R., Gold, R. E., Gotwols, B., et al. (2007). The Mercury dual imaging System on the MESSENGER spacecraft. Space Science Reviews, 131(1–4), 247–338. https://doi.org/10.1007/s11214-007-9266-3

BARRAUD ET AL. 8 of 10

Acknowledgments

O. Barraud thanks the Alexander Von Humboldt Foundation for its financial support. The authors thank Deborah Domingue and two anonymous reviewers for their fruitful revisions. Open Access funding enabled and organized by Projekt DEAL.

- Helbert, J., Maturilli, A., & D'Amore, M. (2013). Visible and near-infrared reflectance spectra of thermally processed synthetic sulfides as a potential analog for the hollow forming materials on Mercury. *Earth and Planetary Science Letters*, 369, 233–238. https://doi.org/10.1016/j.epsl.2013.03.045
- Holsclaw, G. M., McClintock, W. E., Domingue, D. L., Izenberg, N. R., Blewett, D. T., & Sprague, A. L. (2010). A comparison of the ultraviolet to near-infrared spectral properties of Mercury and the Moon as observed by MESSENGER. *Icarus*, 209(1), 179–194. https://doi.org/10.1016/j. icarus.2010.05.001
- Hörz, F., & Cintala, M. (1997). The Barringer Award Address presented 1996 July 25, Berlin, Germany: Impact experiments related to the evolution of planetary regoliths. *Meteoritics & Planetary Sciences*, 32(2), 179–209. https://doi.org/10.1111/j.1945-5100.1997.tb01259.x
- Izenberg, N. R., Klima, R. L., Murchie, S. L., Blewett, D. T., Holsclaw, G. M., McClintock, W. E., et al. (2014). The low-iron, reduced surface of Mercury as seen in spectral reflectance by MESSENGER. *Icarus*, 228, 364–374. https://doi.org/10.1016/j.icarus.2013.10.023
- Kerber, L., Head, J. W., Blewett, D. T., Solomon, S. C., Wilson, L., Murchie, S. L., et al. (2011). The global distribution of pyroclastic deposits on Mercury: The view from MESSENGER flybys 1–3. *Planetary and Space Science*, 59(15), 1895–1909. https://doi.org/10.1016/j.pss.2011. 03.020
- Klima, R. L., Denevi, B. W., Ernst, C. M., Murchie, S. L., & Peplowski, P. N. (2018). Global distribution and spectral properties of low-reflectance material on Mercury. Geophysical Research Letters, 45(7), 2945–2953. https://doi.org/10.1002/2018GL077544
- Klima, R. L., Izenberg, N. R., Murchie, S. L., Meyer, H. M., Stockstill- Cahill, K. R., Blewett, D. T., et al. (2013). Constraining the ferrous iron content of minerals in Mercury's crust. *Lunar Planet. Science*, 44. abstract 1602.
- Lucchetti, A., Pajola, M., Galluzzi, V., Giacomini, L., Carli, C., Cremonese, G., et al. (2018). Mercury hollows as remnants of original bedrock materials and devolatilization processes: A spectral clustering and geomorphological analysis. *Journal of Geophysical Research (Planets)*, 123(9), 2365–2379. https://doi.org/10.1029/2018JE005722
- Lucchetti, A., Pajola, M., Poggiali, G., Semenzato, A., Munaretto, G., Cremonese, G., et al. (2021). Volatiles on Mercury: The case of hollows and the pyroclastic vent of Tyagaraja crater. *Icarus*, 370, 114694. https://doi.org/10.1016/j.icarus.2021.114694
- Lucey, P. G., & Riner, M. A. (2011). The optical effects of small iron particles that darken but do not redden: Evidence of intense space weathering on Mercury. Icarus, 212(2), 451–462. https://doi.org/10.1016/j.icarus.2011.01.022
- McClintock, W. E., Izenberg, N. R., Holsclaw, G. M., Blewett, D. T., Domingue, D. L., Head, J. W., et al. (2008). Spectroscopic observations of Mercury's surface reflectance during MESSENGER's first Mercury flyby. Science, 321(5885), 62–65. https://doi.org/10.1126/science.1159933
- McClintock, W. E., & Lankton, M. R. (2007). The Mercury atmospheric and surface composition spectrometer for the MESSENGER mission. Space Science Reviews, 131(1-4), 481–522. https://doi.org/10.1007/s11214-007-9264-5
- McCord, T. B., & Adams, J. B. (1972a). Mercury: Surface composition from the reflection spectrum. Science, 178(4062), 745–747. https://doi.org/10.1126/science.178.4062.745
- McCord, T. B., & Adams, J. B. (1972b). Mercury: Interpretation of optical observations. *Icarus*, 17(3), 585–588. https://doi.org/10.1016/0019-1035(72)90024-3
- Murchie, S. L., Klima, R. L., Denevi, B. W., Ernst, C. M., Keller, M. R., Domingue, D. L., et al. (2015). Orbital multispectral mapping of Mercury with the MESSENGER Mercury Dual Imaging System: Evidence for the origins of plains units and low-reflectance material. *Icarus*, 254, 287–305. https://doi.org/10.1016/j.icarus.2015.03.027
- Nittler, L., Chabot, N., Grove, T., & Peplowski, P. (2018). The chemical composition of Mercury. In S. Solomon, L. Nittler, & B. Anderson (Eds.), Mercury: The view after MESSENGER (Cambridge planetary science) (pp. 30–51). Cambridge University Press. https://doi.org/10.1017/9781316650684.003
- Nittler, L. R., Starr, R. D., Weider, S. Z., McCoy, T. J., Boynton, W. V., Ebel, D. S., et al. (2011). The major-element composition of Mercury's surface from MESSENGER X-ray spectrometry. Science, 333(6051), 1847–1851. https://doi.org/10.1126/science.1211567
- Noble, S. K., & Pieters, C. M. (2003). Space weathering on Mercury: Implications for remote sensing. Solar System Research, 37(1), 31–35. https://doi.org/10.1023/A:1022395605024
- Noble, S. K., Pieters, C. M., & Keller, L. P. (2007). An experimental approach to understanding the optical effects of space weathering. *Icarus*, 192(2), 629–642. https://doi.org/10.1016/j.icarus.2007.07.021
- Pajola, M., Lucchetti, A., Semenzato, A., Poggiali, G., Munaretto, G., Galluzzi, V., et al. (2021). Lermontov crater on Mercury: Geology, morphology and spectral properties of the coexisting hollows and pyroclastic deposits. *Planetary and Space Science*, 195, 105136. https://doi.org/10.1016/j.pss.2020.105136
- Pieters, C. M., Fischer, E. M., Rode, O., & Basu, A. (1993). Optical effects of space weathering: The role of the finest fraction. *Journal of Geophysical Research*, 98(E11), 20817–20824. https://doi.org/10.1029/93JE02467
- Pieters, C. M., & Noble, S. K. (2016). Space weathering on airless bodies. Journal of Geophysical Research: Planets, 121(10), 1865–1884. https://doi.org/10.1002/2016JE005128
- Robinson, M. S., Murchie, S. L., Blewett, D. T., Domingue, D. L., Hawkins, S. E., III, Head, J. W., et al. (2008). Reflectance and color variations on Mercury: Regolith processes and compositional heterogeneity. *Science*, 321(5885), 66–69. https://doi.org/10.1126/science.1160080
- Thomas, R. J., Rothery, D. A., Conway, S. J., & Anand, M. (2014a). Hollows on Mercury: Materials and mechanisms involved in their formation. *Icarus*, 229, 221–235. https://doi.org/10.1016/j.icarus.2013.11.018
- Thomas, R. J., Rothery, D. A., Conway, S. J., & Anand, M. (2014b). Mechanisms of explosive volcanism on Mercury: Implications from its global distribution and morphology. *Journal of Geophysical Research: Planets*, 119(10), 2239–2254. https://doi.org/10.1002/2014je004692
- Trang, D., Lucey, P. G., & Izenberg, N. R. (2017). Radiative transfer modeling of MESSENGER VIRS spectra: Detection and mapping of submicroscopic iron and carbon. *Icarus*, 293, 206–217. https://doi.org/10.1002/2014JE004692
- Varatharajan, I., Maturilli, A., Helbert, J., Alemanno, G., & Hiesinger, H. (2019). Spectral behavior of sulfides in simulated daytime surface conditions of Mercury: Supporting past (MESSENGER) and future missions (BepiColombo). Earth and Planetary Science Letters, 520, 127– 140. https://doi.org/10.1016/j.epsl.2019.05.020
- Vilas, F. (1985). Mercury: Absence of crystalline Fe2+ in the regolith. *Icarus*, 64(1), 133–138. https://doi.org/10.1016/0019-1035(85)90044-2 Vilas, F., Domingue, D. L., Helbert, J., D'Amore, M., Maturilli, A., Klima, R. L., et al. (2016). Mineralogical indicators of Mercury's hollows composition in MESSENGER color observations. *Geophysical Research Letters*, 43(4), 1450–1456. https://doi.org/10.1002/2015GL067515
- Wang, Y., Xiao, Z., Chang, Y., & Cui, J. (2020). Lost volatiles during the formation of hollows on Mercury. *Journal of Geophysical Research:* Planets, 125(9), e2020JE006559. https://doi.org/10.1029/2020je006559
- Weider, S. Z., Nittler, L. R., Starr, R. D., Crapster-Pregont, E. J., Peplowski, P. N., Denevi, B. W., et al. (2015). Evidence of geochemical terranes on Mercury: Global mapping of major elements with MESSENGER's X-Ray Spectrometer. *Earth and Planetary Science Letters*, 416, 109–120. https://doi.org/10.1016/j.epsl.2015.01.023

BARRAUD ET AL. 9 of 10



# **Geophysical Research Letters**

10.1029/2024GL113933

Weider, S. Z., Nittler, L. R., Starr, R. D., McCoy, T. J., & Solomon, S. C. (2014). Variations in the abundance of iron on Mercury's surface from MESSENGER X-Ray Spectrometer observations. *Icarus*, 235, 170–186. https://doi.org/10.1016/j.icarus.2014.03.002

Weider, S. Z., Nittler, L. R., Starr, R. D., McCoy, T. J., Stockstill-Cahill, K. R., Byrne, P. K., et al. (2012). Chemical heterogeneity on Mercury's surface revealed by the MESSENGER X-Ray Spectrometer. *Journal of Geophysical Research*, 117(E12), E00L05. https://doi.org/10.1029/2012JE004153

BARRAUD ET AL. 10 of 10